Journal of the Serbian Chemical Society
JSCS-info@shd.org.rs • www.shd.org.rs/JSCS
J. Serb. Chem. Soc. 83 (5) 593–609 (2018)
JSCS–5098
UDC 544.654.2:546.57'98–034+543.552+543.42
Original scientific paper

Electrochemical deposition and characterization of AgPd alloy layers

NEVENKA R. ELEZOVIĆ[1#], PIOTR ZABINSKI[2], MILA N. KRSTAJIĆ PAJIĆ[3#], TOMASZ TOKARSKI[4], BORKA M. JOVIĆ[1#] and VLADIMIR D. JOVIĆ[1]*

[1]*Institute for Multidisciplinary Research University of Belgrade, Kneza Višeslava 1, 11030 Belgrade, Serbia,* [2]*AGH University of Science and Technology, Faculty of Non-Ferrous Metals, Al. Mickiewicza 30, 30-059 Krakow, Poland,* [3]*Faculty of Technology and Metallurgy University of Belgrade, Karnegijeva 4, 11000 Belgrade, Serbia and* [4]*AGH University of Science and Technology, Academic Centre for Materials and Nanotechnology, Al. Mickiewicza 30,30-059 Krakow, Poland*

(Received 3 November, revised and accepted 25 December 2017)

Abstract: The AgPd alloys were electrodeposited onto Au and glassy carbon disc electrodes from the solution containing 0.001 mol dm^{-3} $PdCl_2$ + 0.04 mol dm^{-3} AgCl + 0.1 mol dm^{-3} HCl + 12 mol dm^{-3} LiCl under the non-stationary diffusion (quiescent electrolyte) and convective diffusion (ω = 1000 rpm) to the different amounts of charge and at different current densities. Electrodeposited alloy layers were characterized by the anodic linear sweep voltammetry (ALSV), scanning electron microscopy, energy dispersive X-ray spectroscopy (EDS) and X-ray photoelectron spectroscopy (XPS). The compositions of the AgPd alloys determined by the EDS were almost identical to the theoretically predicted ones, while the compositions obtained by XPS and ALSV analysis were similar to each other, but different from those obtained by EDS. Deviation from the theoretically predicted values (determined by the ratio j_L(Pd)/j(Ag)) was more pronounced at lower current densities and lower charges of AgPd alloys electrodeposition, due to the lower current efficiencies for alloys electrodeposition. The ALSV analysis indicated the presence of Ag and Pd, expressed by two ALSV peaks, and in some cases the presence of the additional peak, which was found to correspond to the dissolution of large AgPd crystals, formed at thicker electrodeposits (higher electrodeposition charge), indicating, for the first time, that besides the phase structure, the morphology of alloy electrodeposit could also influence the shape of the ALSV response. In addition to Ag and Pd, the XPS analysis confirmed the presence of AgCl at the surface of samples electrodeposited to low thicknesses (amounts of charge).

Keywords: AgPd alloys electrodeposition; ALSV; XPS; EDS; SEM.

* Corresponding author. E-mail: vladajovic@imsi.bg.ac.rs
# Serbian Chemical Society member.
https://doi.org/10.2298/JSC171103011E

INTRODUCTION

The possibility of AgPd alloys electrodeposition from the solution containing high concentration of chloride ions (12 mol dm^{-3} LiCl) was first mentioned by Brenner,[1] considering the results obtained by Graham *et al.*[2,3] for the electrodeposition of AgPt alloys. It was shown later[4–7] that in the excess of chloride ions AgCl could dissolve to the concentrations sufficient for the electrodeposition of AgPd alloys, with Pd electrodeposition starting at more positive potentials than Ag.

In our previous work,[7] AgPd alloys were characterized by the anodic linear sweep voltammetery (ALSV) technique, indicating the possibility of the formation of an additional phase in the electrodeposited alloys, as a consequence of the appearance of additional peak on the ALSV responses. These investigations were in accordance with some other work,[8] where the measurement of microhardness and the specific electric resistivity indicated the possibility of the formation of ordered structures (or intermetallic compounds) with the approximate stoichiometric compositions of Ag_2Pd_3 and AgPd in the AgPd alloys below 1200 °C, while all of the data found in the binary alloys literature[9] claimed that the AgPd alloy consists of a homogeneous solid solution phase over the entire composition range.

Müller *et al.*[10] conducted an unbiased search of fcc-based $Ag_{1-x}Pd_x$ structures consisting of up to many thousand atoms by using a mixed-space cluster expansion (MSCE). They found an unsuspected ground state at 50–50 % composition – the $L1_1$ structure, currently known in binary metallurgy only for the $Cu_{0.5}Pt_{0.5}$ alloy system. They also provided predicted short-range-order profiles and mixing enthalpies for the high temperature, disordered alloy. Using MSCE they predicted the existence of following ordered structures in the system AgPd: Ag_3Pd, Ag_2Pd, AgPd, Ag_2Pd_2, Ag_3Pd_3, $AgPd_2$ and $AgPd_3$.

In this work, an attempt was made to characterize AgPd alloy layers, electrodeposited from high concentration chloride solutions, by different techniques and compare their results, with the intention to define the appearance of the additional peak on the ALSV responses.

EXPERIMENTAL

All experiments of the AgPd alloys electrodeposition and ALSV analysis were performed in standard electrochemical cells at the temperature of 333±1 K using rotating Au and glassy carbon (GC) disc electrodes (d = 5 mm) and CTV 101 speed control unit (Radiometer Analytical, S.A.). The AgPd alloys were electrodeposited onto Au and GC disc electrodes from the solution containing 0.001 mol dm^{-3} $PdCl_2$ + 0.04 mol dm^{-3} AgCl + 0.1 mol dm^{-3} HCl + 12 mol dm^{-3} LiCl under the conditions of non-stationary diffusion (quiescent electrolyte) and the convective diffusion (ω = 1000 rpm) to the different amounts of charge (0.05 to 3.0 C cm^{-2}), at a constant current density and at various current densities (–0.178 to –0.415 mA cm^{-2}) to the constant amount of charge (0.2 C cm^{-2}). Pure Pd and Ag samples were electrodeposited onto the Au disc electrode from the solutions of 0.04 mol dm^{-3} $PdCl_2$ + 0.1 mol dm^{-3} HCl + 12 mol dm^{-3} LiCl and 0.04 mol dm^{-3} AgCl + 0.1 mol dm^{-3} HCl + 12 mol dm^{-3} LiCl, respectively,

under the conditions of non-stationary and convective diffusion. The dissolution of all coatings by the ALSV technique was performed in another cell containing 0.1 mol dm^{-3} HCl + 12 mol dm^{-3} LiCl under the conditions of convective diffusion (ω = 1000 rpm) at the same temperature of 333±1 K. The alloy samples for the ALSV analysis were electrodeposited onto the Au disc electrode, while those for EDS and XPS analysis were electrodeposited onto GC electrode.

All solutions were made from the extra pure UV water (18.2 MΩ cm), Smart2PureUV, TKA, and p.a. chemicals ($PdCl_2$, AgCl, LiCl, HCl), Sigma–Aldrich.

The saturated calomel electrode (SCE), Radiometer Analytical, was used as the reference electrode in all measurements, while the Platinum mesh (Pt mesh), placed parallel to the working electrode, was used as a counter electrode in both cells. All potentials in the paper are referred at SCE scale.

The *j–E* curves for Ag, Pd and AgPd alloys electrodeposition and the ALSV responses for their dissolution were recorded using the potentiostat Reference 600 and the software PHE 200 and DC 105 (Gamry Instruments). Before the each experiment all solutions were purged with N_2 (5.0 purity) for 30 min. The rotating disc electrodes were polished with the emery papers 1200–4000 and the alumina polishing slurries (1, 0.3 and 0.05 μm) before the electrodeposition of each sample.

The SEM–EDS characterization of all coatings was performed with FEI Versa 3D field emission gun (FEG)-SEM equipped with the energy dispersive spectrometer (EDS).

The XPS analysis of samples was carried out in the ultrahigh vacuum system (3×10^{-10} mbar) equipped with the hemispherical analyzer (SES R4000, Gammadata Scienta). The MgKα source of the incident energy of 1256.6 eV was applied to generate the core excitation. The spectrometer was calibrated according to ISO 15472:2001. The energy resolution of the system, measured at full width at half maximum for Ag $3d_{5/2}$ excitation line, was 0.9 eV. The analysis area of the prepared sample was about 3 mm^2. No gas release and no changes in the sample composition were observed during the measurements. The CasaXPS 2.3.12 software was applied for the analysis of the XPS spectra. No charging was observed for the studied sample, therefore no additional calibration of the spectra energy scale was applied. In the spectra, the background was approximated by a Shirley profile. The spectra deconvolution into a minimum number of components was done by the application of the Voigt-type line shapes (70:30 Gaussian/Lorentzian product). The analytic depth of the XPS method was estimated as 10.2 nm. The calculations were performed with the QUASES-IMFP-TPP2M, ver. 2.2, software according to an algorithm proposed by Tanuma *et al.*[11] This estimation takes into account 95 % of photoelectrons escaping from the surface. The experimental error of the XPS analysis was ±3 %.

RESULTS AND DISCUSSION

Electrodeposition of samples for the ALSV, XPS and EDS analysis

AgPd alloys electrodeposited under the conditions of non-stationary diffusion. The polarization, *j–E* curves, for the electrodeposition of pure Ag, pure Pd and AgPd alloys, onto the Au disc electrode, recorded at a sweep rate of 1 mV s^{-1} and ω = 0 rpm, are presented in Fig. 1. The electrodeposition of Pd is characterized with the well-defined diffusion limiting current density (j_L(Pd)) in the solution containing only $PdCl_2$ ($PdCl_4^{2-}$), as well as in the solution containing $PdCl_2$ and AgCl ($AgCl_4^{3-}$), with the one recorded in the presence of AgCl being

slightly higher (j_L(Pd) = –59.18 μA cm^{-2}). In the absence of AgCl, the sharp peak corresponding to the formation of Pd–H[6,12,13] is detected at –0.10 V, while in the presence of AgCl such peak does not exist, indicating that the Pd–H cannot be formed during the AgPd alloy electrodeposition. Electrodeposition of Ag is seen to commence at about –0.11 V, being characterized with the sharp increase of the current density until the peak at about –0.15 V has been reached. The *j*–*E* curve for AgPd alloy electrodeposition practically represents the sum of those for Pd and Ag. The current density values for AgPd alloy electrodeposition are marked in the figure as $j(1) = 3j_L(\mathrm{Pd})$, $j(2) = 5j_L(\mathrm{Pd})$ and $j(3) = 7j_L(\mathrm{Pd})$.

The composition of the AgPd alloy could be calculated from the parameters of each metal electrodeposition. Masses of the electrodeposited Pd (G_{Pd}) and Ag (G_{Ag}) are given as:

$$G_{\mathrm{Pd}} = \frac{j_{\mathrm{L}}(\mathrm{Pd})tM_{\mathrm{Pd}}S}{zF} \tag{1}$$

$$G_{\mathrm{Ag}} = \frac{j(\mathrm{Ag})tM_{\mathrm{Ag}}S}{zF} \tag{2}$$

where: j_L(Pd) is the diffusion limiting current density for Pd electrodeposition; t is the time of electrodeposition; M_{Pd} is the molecular weight of Pd; S is the electrode surface area; z is the number of exchanged electrons; F is the Faraday's constant; j_d is the current density for the AgPd alloy electrodeposition; j(Ag) is the current density for the Ag electrodeposition ($j(\mathrm{Ag}) = j_d - j_L(\mathrm{Pd})$); M_{Ag} is the molecular weight of Ag.

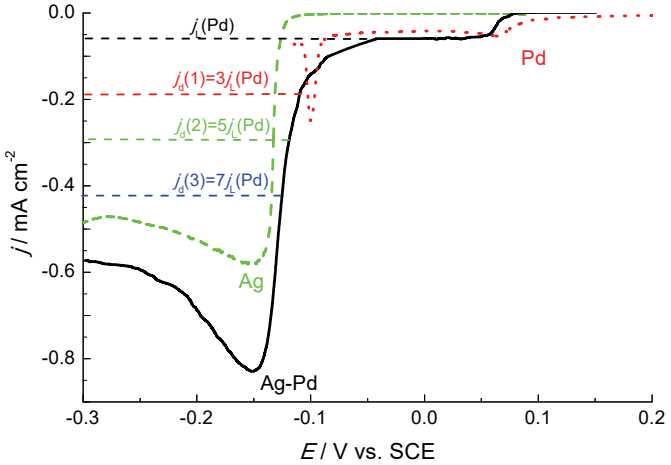

Fig. 1. The *j*–*E* curves for electrodeposition of pure Ag (dashed green line), pure Pd (dotted red line) and AgPd alloy (solid black line), recorded at a sweep rate of 1 mV s^{-1} from the following solutions: (Ag) – 0.04 mol dm^{-3} AgCl + 0.1 mol dm^{-3} HCl + 12 mol dm^{-3} LiCl; (Pd) – 0.001 mol dm^{-3} $PdCl_2$ + 0.1 mol dm^{-3} HCl + 12 mol dm^{-3} LiCl; (AgPd) – 0.001 mol dm^{-3} $PdCl_2$ + 0.04 mol dm^{-3} AgCl + 0.1 mol dm^{-3} HCl + 12 mol dm^{-3} LiCl.

The composition of the AgPd alloy expressed as a mass share of each metal is obtained from the following equations:

$$w(\mathrm{Pd}) = \frac{G_{\mathrm{Pd}}}{G_{\mathrm{Pd}} + G_{\mathrm{Ag}}} \tag{3}$$

$$w(\mathrm{Ag}) = \frac{G_{\mathrm{Ag}}}{G_{\mathrm{Pd}} + G_{\mathrm{Ag}}} \tag{4}$$

These equations, presenting the mass share of metals, are practically identical to the atomic share of metals, since the molecular weights of both metals are very close. Using Eqs. (1)–(4) the AgPd alloy compositions for the different current densities and the constant charge (Q = 0.2 C cm^{-2}) were calculated and presented in Fig. 2 as a function of the current density for the alloy electrodeposition, j_d (□, ●). It can be seen that the content of both metals (at.%) changes exponentially with the increase of the current density, starting from j_L(Pd). The amount of Pd decreases, while the amount of Ag increases and already at $j_d = 1.5j_L$(Pd) the equal amounts of Ag and Pd should be electrodeposited.

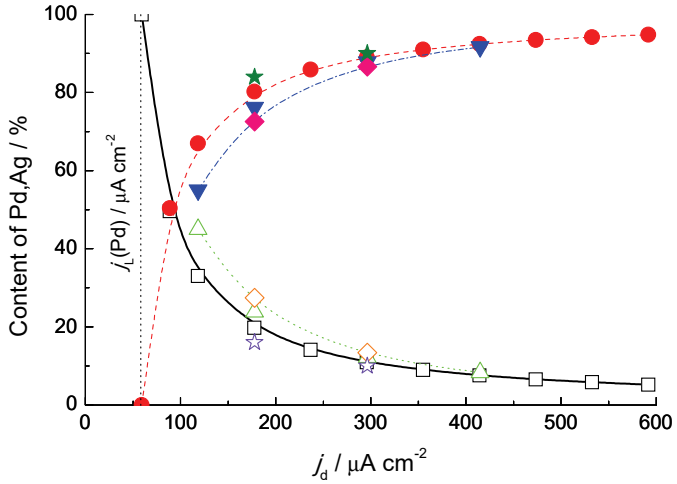

Fig. 2. Composition of the AgPd alloys (at.%) calculated from Eqs. (1)–(4): (□) Pd; (●) Ag. Composition of AgPd alloys obtained by different techniques: (△) Pd and (▼) Ag obtained from the ALSV; (◇) Pd and (◆) Ag obtained from the XPS; (☆) Pd and (★) Ag obtained from the EDS (see Tables S-I–S-III of the Supplementary material to this paper).

AgPd alloys electrodeposited under the conditions of convective diffusion. In the case of pure Pd electrodeposition from the solution containing 0.001 mol dm^{-3} $PdCl_2$ + 0.1 mol dm^{-3} HCl + 12 mol dm^{-3} LiCl under the conditions of the convective diffusion, the diffusion limiting current density for Pd cannot be precisely defined, as it is shown in Fig. 3a. Although the commencement of Pd electro-

deposition is moved to slightly more cathodic potentials in comparison with that at non-stationary diffusion (Fig. 1), a well-defined plateau of the j_L(Pd) does not exist at any applied rotation rate. A sharp peak of the Pd–H formation appears at the same potential (about –0.10 V), as in the case of the non-stationary diffusion. The reason for such behaviour might be that the sweep rate of 1 mV s^{-1} is faster than the one which is necessary for the Pd electrodeposition. An attempt was made to apply the sweep rate of 0.1 mV s^{-1}, but with that sweep rate the plateau of the diffusion limiting the current density could be obtained only at 400 rpm, while at higher ω values such plateau could not be detected. Taking into account that at ω = 900 rpm the diffusion limiting current density for Pd electrodeposition is 10 times higher than that for the non-stationary diffusion (see Figs. 1 and 3a) the amount of the electrodeposited Pd is 10 times higher and in the region of the plateau of the diffusion limiting current density the electrodeposit becomes rougher with the increasing cathodic potential producing the increase of the j_L(Pd), due to the increase of the real surface area. This increase is more pronounced than in the case of the non-stationary diffusion and j_L(Pd) cannot be well-defined.

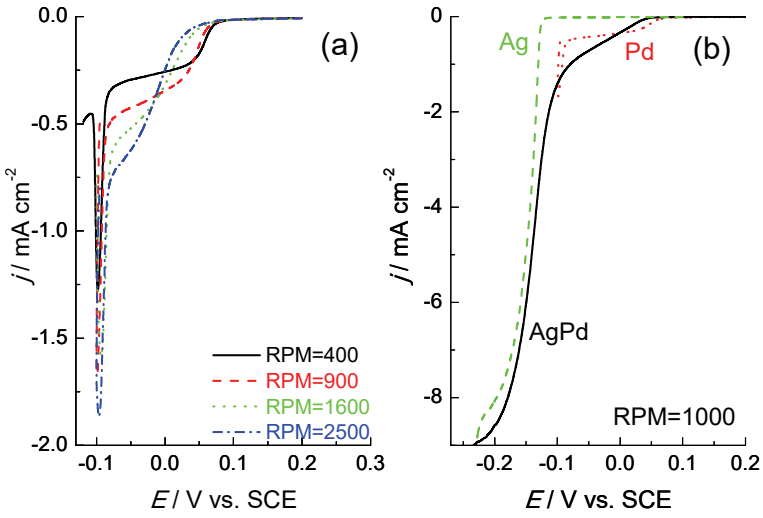

Fig. 3. a) The *j–E* curves for electrodeposition of pure Pd recorded at a sweep rate of 1 mV s^{-1} and different ω (given in the figure) form the solution 0.001 mol dm^{-3} $PdCl_2$ + 0.1 mol dm^{-3} HCl + 12 mol dm^{-3} LiCl. b) The *j–E* curves for electrodeposition of pure Ag (green dashed line), pure Pd (red dotted line) and AgPd alloy (black solid line), recorded at the sweep rate of 1 mV s^{-1} and ω = 1000 rpm, form the following solutions: (Ag) – 0.04 mol dm^{-3} AgCl + 0.1 mol dm^{-3} HCl + 12 mol dm^{-3} LiCl; (Pd) – 0.001 mol dm^{-3} $PdCl_2$ + 0.1 mol dm^{-3} HCl + 12 mol dm^{-3} LiCl; (AgPd) – 0.001 mol dm^{-3} $PdCl_2$ + 0.04 mol dm^{-3} AgCl + 0.1 mol dm^{-3} HCl + 12 mol dm^{-3} LiCl.

For the AgPd alloy electrodeposition in the solution 0.001 mol dm^{-3} $PdCl_2$ + 0.04 mol dm^{-3} AgCl + 0.1 mol dm^{-3} HCl + 12 mol dm^{-3} LiCl the situation is even

worse. The current density of the Pd electrodeposition increases in the potential range where a plateau is expected, as seen in Fig. 3b (black solid line). As in the case of non-stationary diffusion, the electrodeposition of Ag commences at the same potential, characterized with the sharp increase of the current density. Hence, the calculation of the alloy composition using Eqs. (1)–(4) is impossible and the composition must be determined by other techniques, such as ALSV, XPS or EDS.

Characterization of electrodeposited AgPd alloys by the ALSV technique

The samples for the ALSV analysis were electrodeposited onto the Au disc electrode, due to the reasons explained in our previous work.[7]

Characterization of AgPd alloys electrodeposited under the conditions of non-stationary diffusion. The typical ALSV responses[14] for the dissolution of AgPd alloys electrodeposited under the conditions of non-stationary diffusion (Fig. 1) are shown in Fig. 4a, for the samples electrodeposited at different j_d (Q_d = 0.2 C cm^{-2}) and in Fig. 4b, for the samples electrodeposited to different Q_d (j_d = –178 μA cm^{-2}).

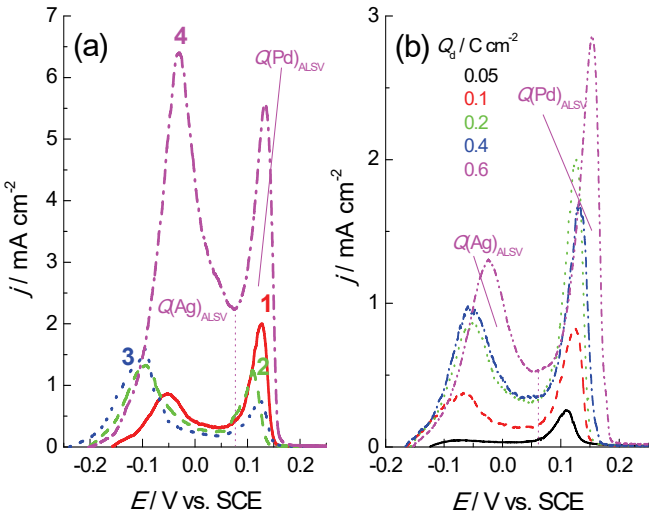

Fig. 4. ALSV responses for dissolution of AgPd alloys recorded at ω = 1000 rpm and a sweep rate of 1 mV s^{-1} in the solution containing 0.1 mol dm^{-3} HCl + 12 mol dm^{-3} LiCl. a) Alloys electrodeposited to the charge Q_d = 0.2 C cm^{-2} at different current densities: (1) $j_d(1) = 3j_L$(Pd) = –178 μA cm^{-2}; (2) $j_d(2) = 5j_L$(Pd) = –296 μA cm^{-2}; (3) $j_d(3) = 7j_L$(Pd) = –415 μA cm^{-2}; (4) $j_d(4) = 5j_L$(Pd) = –296 μA cm^{-2}; Q_d = 1.0 C cm^{-2}. b) Alloys electrodeposited to different charges (given in the figure) at a constant current density j_d = –178 μA cm^{-2}.

Considering these ALSV responses, it seems that all of them are characterized with two dissolution peaks, one corresponding to the dissolution of Ag and one corresponding to the dissolution of Pd. With the increase of the amount

of charge for AgPd alloy electrodeposition (thickness of the alloy layer), the peak current densities on the ALSV responses become higher. In order to determine approximate composition of the AgPd alloys (taking into account high values of current efficiencies for alloy electrodeposition, see Tables S-I–S-III), the ALSV responses were analyzed as schematically presented in Fig. 4a for the sample 4, as well as in Fig. 4b for the sample corresponding to the dissolution of AgPd alloy electrodeposited to $Q_d = 0.6$ C cm^{-2} (see also Fig. 5b). The ALSV responses were divided in two parts, the one corresponding to the dissolution of Ag ($Q(\mathrm{Ag})_{\mathrm{ALSV}}$) and the another one corresponding to the dissolution of Pd ($Q(\mathrm{Pd})_{\mathrm{ALSV}}$). The at.% of Pd and Ag, calculated from their charges on the ALSV responses, are presented in Fig. 2 (△ and ▼, respectively), while the calculated percentages are presented with □ for Pd and ● for Ag. The percentages of Pd and Ag obtained from the XPS analysis are presented with ◇ for Pd and ◆ for Ag, while those obtained from the EDS analysis are presented with ☆ for Pd and ★ for Ag, respectively. It should be stated here that only two samples presented in the Fig. 2 were analyzed by the XPS and EDS (see Table S-I). The results of the composition analysis with all three techniques were different (Tables S-I–S-III). Relatively good agreement was obtained for those obtained from the XPS and ALSV analysis, where the at.% Pd was the lowest for sample AgPd2. The difference between the calculated percentages of Pd (□) and Ag (●) and those determined from their charges on the ALSV responses (Pd (△), Ag (▼)), as well as those determined by XPS (Pd(◇), Ag(◆)), have increased with the decrease of the electrodeposition current density. Actually, for the ALSV and XPS analysis, the increase in the at.% Pd is equal to the decrease in the at.% Ag. Taking into account that the results of XPS and ALSV analysis are in relatively good agreement, the difference between the theoretically predicted and the experimentally detected alloy compositions could be the consequence of lower current efficiency for the alloy electrodeposition at lower current densities (j_d) and lower amounts of charge for alloy electrodeposition (Q_d) (see Tables S-I and S-II). At higher current densities (< –400 μA cm^{-2}) and higher values of Q_d the current efficiency η_j for alloy electrodeposition is very high (> 97 %), causing the identical theoretical and experimentally determined compositions of AgPd alloys (see Fig. 2 and Tables S-I and S-II). Due to the low current densities for AgPd alloys electrodeposition, the highest amount of charge was $Q_d = 1.5$ C cm^{-2} (see Table S-I, sample (5)).

Characterization of AgPd alloys electrodeposited under the conditions of convective diffusion. ALSV responses for the dissolution of AgPd alloys electrodeposited under the conditions of the convective diffusion are shown in Fig. 5a for samples electrodeposited at different j_d ($Q_d = 0.2$ C cm^{-2}) and in Fig. 5b for the sample electrodeposited at $j_d = -7.0$ mA cm^{-2} to the $Q_d = 3.0$ C cm^{-2}. For the dis-

solution of these samples the same comments and conclusions as those for the samples electrodeposited under the conditions of non-stationary diffusion are valid.

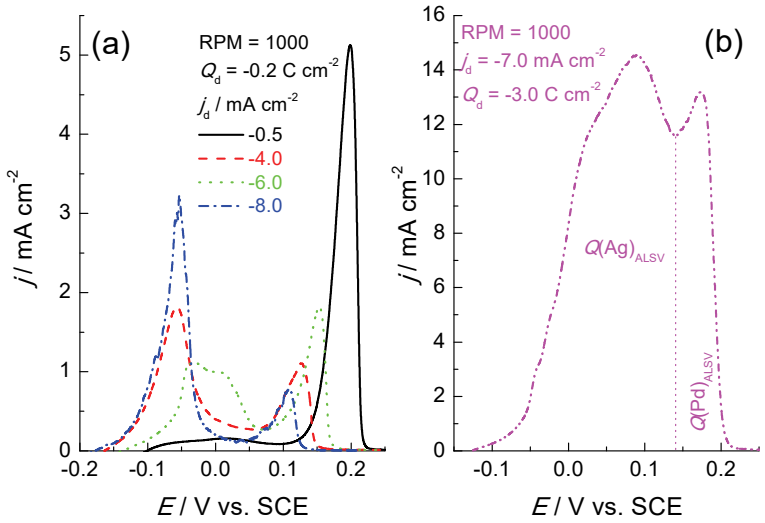

Fig. 5. ALSV responses for dissolution of AgPd alloys recorded at ω = 1000 rpm and a sweep rate of 1 mV s^{-1} in the solution 0.1 mol dm^{-3} HCl + 12 mol dm^{-3} LiCl. a) Alloys electrodeposited to the charge Q_d = - 0.2 C cm^{-2} at different current densities (marked in the figure). b) Alloy electrodeposited to the highest amount of charge.

With the increase of j_d the peak of the Ag dissolution increases, while the peak of the Pd dissolution decreases (Fig. 5a), as in the case of the samples electrodeposited under the conditions of non-stationary diffusion. For the samples electrodeposited under the conditions of the convective diffusion the peak potential of Pd dissolution has become more negative with the increase of j_d (Fig. 5a), while the one for the samples electrodeposited under the conditions of the non-stationary diffusion remains practically the same (Fig. 4a). Such behaviour could be the result of the different morphology of AgPd samples electrodeposited by these two procedures (see Figs. 9–11). For the sample electrodeposited to the highest charge (Q_d = 3.0 C cm^{-2}), the separation of Ag and Pd peaks is not as well defined as for samples electrodeposited to the lower charges.

Only one sample (ALSV presented in Fig. 5b) was analyzed by the XPS and EDS. The results of conditions for AgPd alloy electrodeposition and their compositions are shown in Table III.

Procedure of fitting ALSV responses. According to the theoretical predictions for the ALSV technique,[14] ALSV responses of the solid solution type alloys should be characterized with the two separate peaks only (corresponding to the dissolution of each metal), since in the case of alloys with the intermediate phases (intermetallic compounds) each phase should be characterized with a sep-

arate peak on the ALSV. The shape of the ALSV responses of AgPd alloys is seen to change from ALSV responses with two peaks only to the ALSV responses with more than two peaks, depending on the value of j_d and Q_d (see Figs. 4 and 5). The procedure of fitting ALSV responses with two peaks (using Origin multi-peaks Lorentzian function – Origin 8.0, OriginLab, USA) was possible only for the samples electrodeposited at smaller current densities (< 200 μA cm^{-2}) and the samples electrodeposited to the cathodic charges lower than 0.4 C cm^{-2}. In Fig. 6 are presented results of fitting the ALSV responses of the AgPd alloys dissolution electrodeposited at different values of j_d to a different Q_d under the conditions of the non-stationary diffusion. The fitting lines (black solid lines) are in a good agreement with the experimental ones (the magenta dash-dot-dot lines), with the Ag peak being labelled with the red dash lines, Pd peak with the green dotted lines and a third, unknown peak, UP, whose origin was undefined, was labelled with a blue dash-dot lines. It should be emphasized that the fit of the most positive peak, Pd peak, cannot follow the shape of the Lorentzian peak after the peak maximum has been reached, since the peak current density sharply decreases due to the removal of the traces of the electrodeposit and to the certain discrepancy between the fitting and the experimental lines must exist, as it could be seen in Figs. 6 and 7. As it was already stated, the only sample electrodeposited at $j_d = 3j_L$(Pd) could be fitted with two peaks, Fig. 6a and b, while the appearance of a third peak (UP) could already be observed for the sample electrodeposited at $j_d = 7j_L$(Pd).

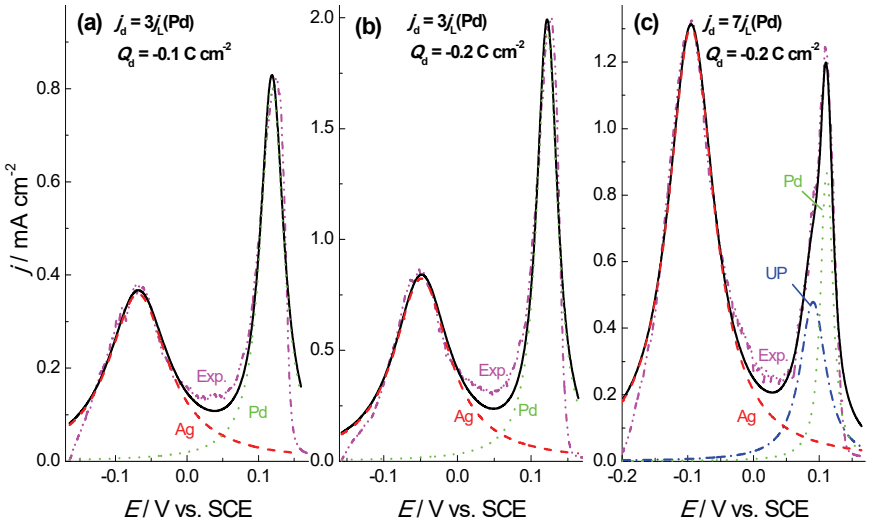

Fig. 6. Results of fitting ALSV responses of the AgPd alloys electrodeposited at $j_d = 3j_L$(Pd), Q_d = 0.1 C cm^{-2} (a), $j_d = 3j_L$(Pd), Q_d = 0.2 C cm^{-2} (b) and $j_d = 7j_L$(Pd), Q_d = 0.2 C cm^{-2} (c). Fitting (black solid lines), experimental (magenta dash-dot-dot lines), Ag (red dashed lines), Pd (green dotted lines), unknown peak (UP) (blue dash-dot lines).

For the AgPd alloys electrodeposited at a constant current density j_d = –178 μA cm^{-2} ($j_d = 3j_L$(Pd)) and ω = 0 rpm to the different amounts of charge (Fig. 4b, Table II), the appearance of a third peak (UP) was detected at the cathodic charges higher than 0.2 C cm^{-2}.

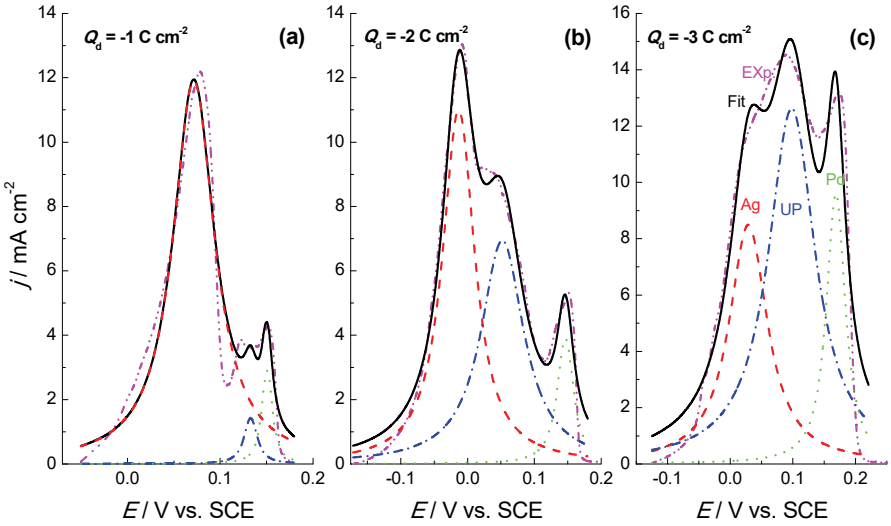

Fig. 7. Results of fitting ALSV responses of the AgPd alloys electrodeposited at ω = 1000 rpm: a) j_d = –5 mA cm^{-2}, Q_d = 1.0 C cm^{-2}; b) j_d = –5 mA cm^{-2}, Q_d = 2.0 C cm^{-2}; c) j_d = –7 mA cm^{-2}, Q_d = 3.0 C cm^{-2}. Fitting (black solid lines), experimental (magenta dash-dot-dot lines), Ag (red dashed lines), Pd (green dotted lines), unknown phase (UP) (blue dash-dot lines).

In addition to the Q(Pd)$_{ALSV}$ and Q(Ag)$_{ALSV}$ in Tables I–III are presented the results obtained by the analysis of the charge under the third peak, Q(UP)$_{ALSV}$, and the whole ALSV responses (Q_{ALSV}). Third peak appears to be more pronounced since its charge, expressed in the percentages of the total charge under the ALSV (Q_{ALSV}), increases with the rise of the cathodic current density and the cathodic charge. It should be stated that such approach is a rough approximation, since all three peaks obtained by the fitting procedure overlap and it is practically not possible to determine the exact amount of charge for the UP peak.

In Fig. 7 are presented the ALSV responses of AgPd alloy layers electrodeposited at various current densities and the various amounts of charge under the conditions of convective diffusion (ω = 1000 rpm). Since the cathodic charges are higher than 0.4 C cm^{-2} all ALSV responses had to be fitted with three peaks. The UP peak is seen to increase with the increase of Q_d.

The results presented in Table III are obtained by the analysis of ALSV responses shown in Fig. 7. As it can be seen, the charge for UP reaches high values in the samples electrodeposited to higher cathodic charges (Q_d = 2.0 and 3.0 C

cm^{-2}). The composition of only one sample (AgPd3, Q_d = 3.0 C cm^{-2}) was analyzed by the XPS and EDS techniques.

Hence, considering the results of the ALSV analysis it appears that all electrodeposited AgPd alloy layers do not represent solid the solution type alloy, being characterized with the presence of two peaks only (corresponding to the dissolution of Ag and Pd). The appearance of a UP peak could be either the consequence of the formation of an additional phase, or the properties of the AgPd electrodeposit. Theoretically, there is a possibility for the formation of the different ordered structures in the AgPd system,[10] but the question arises, is it possible to detect these ordered structures by the application of the ALSV technique. In order to define the appearance of UP peak on the ALSV responses, the additional analysis, using XPS and SEM–EDS techniques was performed.

Characterization of the AgPd alloys by the XPS analysis

Five peaks, namely O1s, Ag3d, Pd3d, C1s and Cl2p were detected on the surface of AgPd1, AgPd2 and AgPd3 samples. For the composition analysis the most important peaks are Ag3d and Pd3d and their percentages were taken from the complete XPS spectra. The XPS results for these two elements are shown in Fig. 8. By their deconvolution it was discovered that a certain amount of AgCl could be detected on the Ag3d spectra. The amount of AgCl was seen to decrease from AgPd1 to AgPd3 samples, being 19.3 % for AgPd1, 16.4 % for AgPd2 and 5.3 % for AgPd3. A certain amount (smaller in percentages than AgCl) of PdO was detected under the Pd3d spectra, was also decreasing from AgPd1 to AgPd3.

Characterization of the AgPd alloys by the EDS analysis

The SEM micrographs for the sample AgPd1 are shown in Fig. 9a and b, while the EDS spectra recorded at the marked surface positions in Fig.9a are presented in the Supplementary material. The surface is heterogeneous and rough, with the presence of white and gray parts and the substrate is not completely covered with the electrodeposit (a,b). EDS analysis of the white parts on the Fig.9a contains approximately 12.6 at.% Cl, while the EDS of gray parts shows only 0.6 at.% Cl, indicating that white parts of the electrodeposit could be AgCl with the excess of chloride since the ratio Ag/Cl is higher than 1. The AgCl was detected on much larger surface area (3 mm^2) and on much lower depth (10.2 nm) by the XPS analysis. Hence, for the EDS analysis only grey parts of the electrodeposit were considered and the corresponding results are given in Tables S-I–S-III. As can be seen in Fig. 9a, AgPd crystals are characterized by the rounded shape with the dimensions of about 200 nm.

The SEM micrographs for sample AgPd2 are presented in Fig. 9c and d, while the EDS spectra recorded at the marked surface positions in Fig.9c are shown in Supplementary material. Again, the surface is heterogeneous and rough,

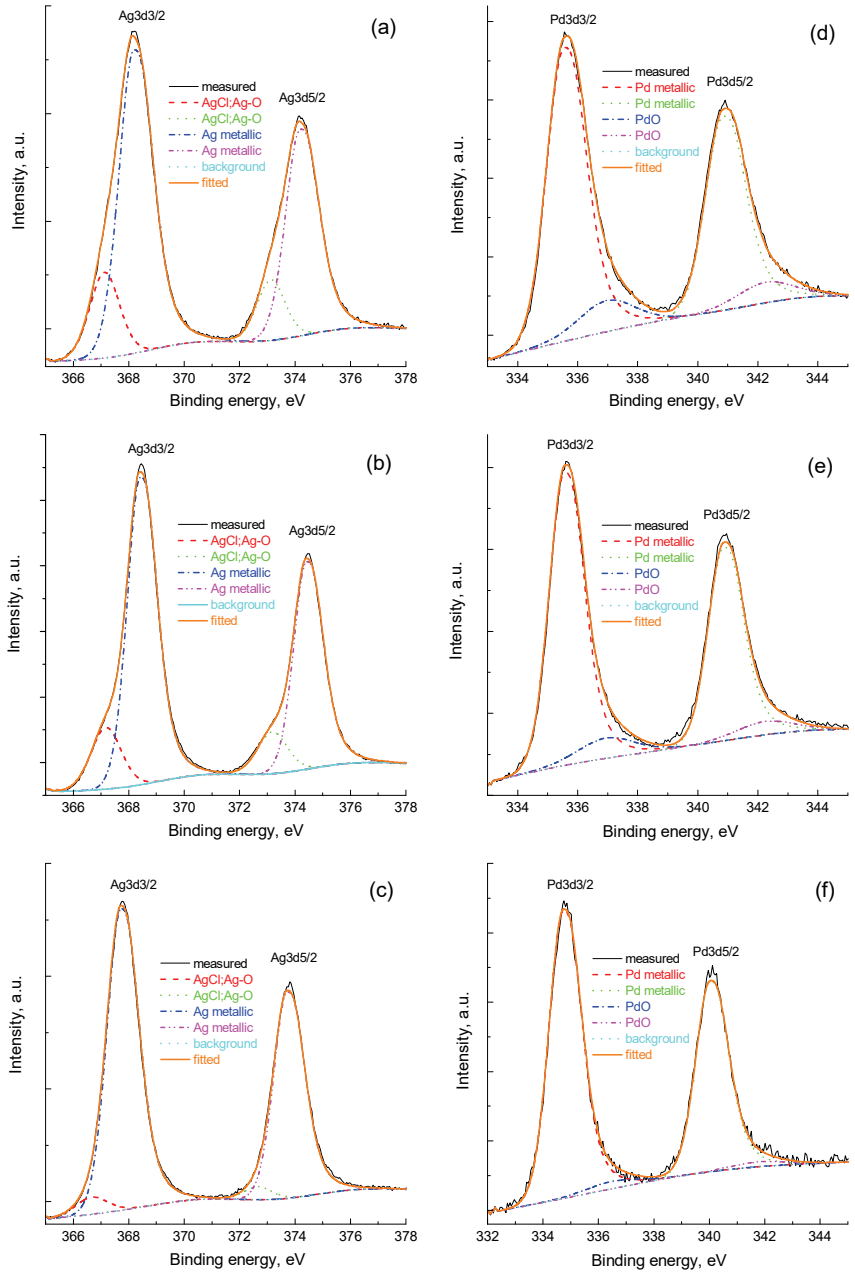

Fig. 8. Results of the XPS analysis for Ag3d (a,b and c) and Pd3d (d,e and f) in samples AgPd1, AgPd2 and AgPd3, respectively.

with the presence of white and grey parts and the substrate is not completely covered with electrodeposit (c,d), but the non-covered substrate surface is smaller

in comparison with that for the sample AgPd1. The white parts on the Fig. 9c contain approximately 13.1 at.% Cl, while the EDS of the grey parts shows only 0.9 at.% Cl. Concerning the presence of AgCl (XPS) on the surface of sample AgPd2, the same conclusion, as that for the sample AgPd1, is valid. The AgPd crystals (Fig. 9c) are characterized by the rounded shape with the dimensions of about 300 nm.

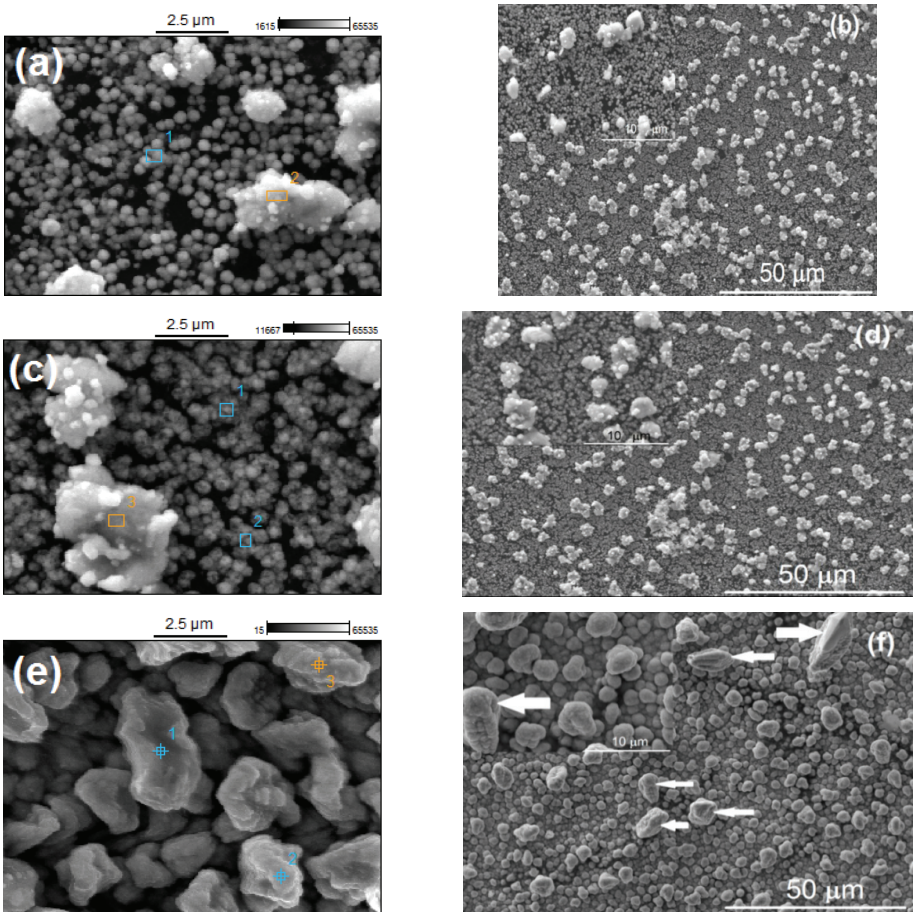

Fig. 9. SEM micrographs of the surface of AgPd layers: a) and b) AgPd1 sample, c) and d) AgPd2 sample and e) and f) AgPd3 sample. On microphotographs a), c) and e) the positions for the EDS analysis are marked (EDS spectra are given in Supplementary material, the average composition given in Table S-I).

The SEM micrographs for the sample AgPd3 are presented in Fig. 9e and f, while the EDS spectra recorded at the marked surface positions in Fig. 9e are shown in Supplementary material. The surface is rough, composed of much larger crystals than those of samples AgPd1 and AgPd2. No presence of white

parts was detected on the sample surface, indicating the absence of AgCl. Since this electrodeposit is much thicker, the substrate is completely covered with the electrodeposit (e,f). At some positions the large AgPd crystals, of about 10–20 μm high (marked with arrows in Fig. 9f), growing normally to the electrode surface, are detected (f), which is typical for the metals with fast nucleation rate, as are Ag and Pd.[15–17]

Considering the results of ALSV, XPS and EDS analysis for the samples electrodeposited under the conditions of the non-stationary diffusion (Fig. 2), it could be stated that the similar compositions obtained by the ALSV and XPS are the result of the analysis of the large sample area (in the case of ALSV the whole sample, in the case of XPS 3 mm^2), taking into account the presence of AgCl on their surfaces. For the EDS analysis only grey parts of the surfaces were analyzed, giving higher percentages of Ag in the electrodeposit (Tables S-I–S-III). It should be mentioned that the average composition is analyzed by ALSV and XPS, while EDS usually presents the local composition – at the specific, chosen surface locations.

The appearance of UP on the ALSV responses, recorded for samples obtained at higher electrodeposition current densities and higher charges, is most probably the consequence of different morphologies. Actually, with the increase of j_d and Q_d the morphology becomes similar to that presented in Fig. 9f and the Ag from large AgPd crystals, particularly those of higher heights (marked with arrows in Fig. 9f), dissolves easier and faster than from the rest of the surface (the dissolution is a pure inversion of deposition).[18] When the whole amount of Ag from the large AgPd crystals is dissolved, the current density on the ALSVs starts to decrease until the Ag begins to dissolve from the rest of the surface, causing the appearance of an additional peak on the ALSV responses. Hence, the appearance of an additional peak could be the consequence of this phenomenon.[15–18] The ALSV response for the thin AgPd alloy layer (Fig. 6a and b – low j_d and Q_d) shows no additional peaks and could be fitted with two peaks using Origin multi-peaks Lorentzian function. Hence, it appears that the additional peak on the ALSV responses is the result of faster dissolution of large crystals of higher heights. This means that $Q(\mathrm{UP})_{\mathrm{ALSV}}$, given in Tables S-I–S-III, roughly represents the percentage of the total surface area containing large AgPd crystals of higher heights.

CONCLUSIONS

The AgPd alloys electrodeposited from the solution containing 0.001 mol dm^{-3} $PdCl_2$ + 0.04 mol dm^{-3} AgCl + 0.1 mol dm^{-3} HCl + 12 mol dm^{-3} LiCl under the conditions of non-stationary (ω = 0 rpm) and the convective diffusion (ω = = 1000 rpm), to the different amounts of charge and at different current densities, were characterized by the ALSV, SEM, EDS and XPS techniques. The compo-

sitions of the AgPd alloys determined by the EDS were almost identical to the theoretically predicted ones, while the compositions obtained by the XPS and the ALSV analysis (they were almost identical) were different. Deviation from the theoretically predicted values (determined by the ratio $j_L(Pd)/j(Ag)$) was more pronounced at lower current densities and at lower charges of AgPd alloys electrodeposition, due to lower current efficiencies for alloys electrodeposition. The ALSV analysis indicated the presence of Ag, Pd, expressed by the two ALSV peaks, and the additional peak, which was found to correspond to the dissolution of large AgPd crystals formed at electrodeposits with higher charge and larger cathodic current densities. The XPS analysis, among the Ag and Pd, confirmed the presence of AgCl at the surface of samples electrodeposited to low amounts of charge.

SUPPLEMENTARY MATERIAL

Additional calculation and SEM–EDS data are available electronically at the pages of the journal website: http://www.shd.org.rs/JSCS/, or from the corresponding author on request.

Acknowledgement. The authors are indebted to the Ministry of Education, Science and Technological Development of the Republic of Serbia (Project No. 172054) for the financial support of this work. The authors would like to acknowledge the COST MP 1407 action for networking support.

ИЗВОД

КАРАКТЕРИЗАЦИЈА ЕЛЕКТРОХЕМИЈСКИ ИСТАЛОЖЕНИХ СЛОЈЕВА СРЕБРО-ПАЛАДИЈУМ ЛЕГУРА РАЗЛИЧИТИМ ТЕХНИКАМА

НЕВЕНКА Р. ЕЛЕЗОВИЋ[1], PIOTR ZABINSKI[2], МИЛА Н. КРСТАЈИЋ ПАЈИЋ[3], TOMASZ TOKARSKI[4], БОРКА М. ЈОВИЋ[1] и ВЛАДИМИР Д. ЈОВИЋ[1]

[1]Институт за мултидисциплинарна истраживања Универзитета у Београду, Кнеза Вишеслава 1, 11030 Београд, [2]AGH University of Science and Technology, Faculty of Non-Ferrous Metals, Al. Mickiewicza 30,30-059 Krakow, Poland, [3]Технолошко–металуршки факултет Универзитета у Београду, Карнегијева 4, 11000 Београд и [4]AGH University of Science and Technology, Academic Centre for Materials and Nanotechnology, Al. Mickiewicza 30,30-059 Krakow, Poland

Танки слојеви сребро–паладијум легура исталожени су електрохемијским поступком на дисковима од злата и стакластог угљеника из раствора 0,001 mol dm^{-3} $PdCl_2$ + 0,04 mol dm^{-3} AgCl + 0,1 mol dm^{-3} HCl + 12 mol dm^{-3} LiCl под условима нестационарне (ω = 0 o min^{-1}) и конвективне (ω = 1000 o min^{-1}) дифузије, при различитим вредностима густине струје таложења и количине наелектрисања. Електрохемијски исталожени слојеви окарактерисани су анодном линеарном волтаметријом (ALSV), скенирајућом електронском микроскопијом (SEM), енергетски диспергованом рендгенском спектроскопијом (EDS) и рендгенском фотоелектронском спектроскопијом (XPS). Састав сребро–паладијум легура одређен EDS техником био је скоро идентичан теоријски предвиђеном, док су састави одређени XPS и ALSV техникама (који су били скори идентични) одступали од теоријски предвиђеног, при чему је то одступање било израженије код узорака исталожених мањим густинама струје и узорака исталожених до мањих количина наелектрисања. ALSV анализа је показала присуство сребра и паладијума, изражено као два струјна врха, као и присуство још једног струјног врха, за који је установљено SEM и EDS анализама да је последица растварања великих сребро–паладијум

кристала који се формирају код дебљих превлака, исталожених до већих количина наелектрисања. На тај начин је по први пут показано да поред фазног састава и морфологија талога легура може утицати на облик ALSV одговора. XPS анализом је на површини тањих узорака (исталожених до мањих количина наелектрисања у условима нестационарне дифузије) потврђено присуство сребро-хлорида, поред сребра и паладијума.

(Примљено 3. новембра, ревидирано и прихваћено 25. децембра 2017)

REFERENCES

1. 1. A. Brenner, *Electrodeposition of Alloys: Principles and Practice*, Academic Press, New York, 1963
2. A. K. Graham, S. Helman, H. L. Pinkerton, *Plating* **35** (1948) 1217
3. A. K. Graham, S. Helman, H. L. Pinkerton, *Plating* **36** (1949) 47
4. U. Cohen, F. B. Koch, R. Sard, *J. Electrochem. Soc.* **130** (1983) 1987
5. U. Cohen, K. R. Walton, R. Sard, *J. Electrochem. Soc*. **131** (1984) 2489
6. V. D. Jović, M. V. Stojanović, B. M. Jović, Lj. Gajić-Krstajić, *J. Serb. Chem. Soc*. **57** (1992) 951
7. V. D. Jović, B. M. Jović, A. R. Despić, *J. Electroanal. Chem*. **357** (1992) 357
8. E. M. Savitskii, N. L. Pravoverov, *Zh. N. Khim*. **76** (1961) 499
9. *ASM Handbook*, *Vol. 3*, *Alloy Phase Diagrams*, 1992 (converted to electronic files in 1998), ASM International, Almere, 1998
10. S. Müller, A. Zunger, *Phys. Rev. Lett*. **87** (2001) 165502-1
11. S. Tanuma, C. J. Powell, D. R. Penn, *Surface Interface Anal*. **21** (1993) 165
12. R. Le. Penven, W. Levason, D. Pletcher, *J. Appl. Electrochem*. **20** (1990) 399
13. R. Le. Penven, W. Levason, D. Pletcher, *J. Appl. Electrochem*. **22** (1992) 421
14. V. D. Jović, U. Č. Lačnjevac, B. M. Jović, in *Modern Aspects of Electrochemistry*, No. 57, S. S. Djokić, Ed., Springer Science + Business Media, New York, 2014, p. 23
15. K. I. Popov, S. S. Djokić, N. D. Nikolić, V. D. Jović, *Morphology of Electrochemically and Chemically Deposited Metals*, Springer International Publishing, Cham, 2016, p. 185
16. B. M. Jović, V. D. Jović, G. Branković, M. Radović, N. V. Krstajić, *Electrochim. Acta* **224** (2017) 571
17. V. M. Kozlov, L. P. Bicelli, *J. Cryst. Growth* **203** (1999) 255
18. G. Wranglen, *Electrochim. Acta* **2** (1960) 130.